Vol. 16, pp. 140–146 (2019)
doi: 10.2142/biophysico.16.0_140

Biophysics and Physicobiology
https://www.jstage.jst.go.jp/browse/biophysico/

*Review Article*

# Cryo-EM studies of the rotary $H^+$-ATPase/synthase from *Thermus thermophilus*

Atsuko Nakanishi[1], Jun-ichi Kishikawa[1], Kaoru Mitsuoka[2] and Ken Yokoyama[1]

[1]*Department of Molecular Biosciences, Kyoto Sangyo University, Kyoto 603-8555, Japan*
[2]*Research Center for Ultra-High Voltage Electron Microscopy, Osaka University, Ibaraki, Osaka 567-0047 Japan*

Received March 29, 2019; accepted August 9, 2019

**Proton-translocating rotary ATPases couple proton influx across the membrane domain and ATP hydrolysis/synthesis in the soluble domain through rotation of the central rotor axis against the surrounding peripheral stator apparatus. It is a significant challenge to determine the structure of rotary ATPases due to their intrinsic conformational heterogeneity and instability. Recent progress of single particle analysis of protein complexes using cryogenic electron microscopy (cryo-EM) has enabled the determination of whole rotary ATPase structures and made it possible to classify different rotational states of the enzymes at a near atomic resolution. Three cryo-EM maps corresponding to different rotational states of the V/A type $H^+$-rotary ATPase from a bacterium *Thermus thermophilus* provide insights into the rotation of the whole complex, which allow us to determine the movement of each subunit during rotation. In addition, this review describes methodological developments to determine higher resolution cryo-EM structures, such as specimen preparation, to improve the image contrast of membrane proteins.**

**Key words:** V-ATPase, rotary motor, ATP synthase

Corresponding author: Atsuko Nakanishi, Department of Molecular Biosciences, Kyoto Sangyo University, Motoyama Kamigamo, Kita-ku, Kyoto 603-8555, Japan.
e-mail: nakani@cc.kyoto-su.ac.jp

ATP produced by ATP synthases is a key molecule for the metabolism of every living organism. ATP synthases belong to a family of enzymes known as rotary ATP synthases and are categorized as F- and V-type ATPases (Fig. 1A, B). They share many structural and mechanistic features, such as mechanochemical coupling of ion translocation and ATP hydrolysis/synthesis through rotation [1–6]. Reactions mediated by rotary ATPases are reversible, and consequently can function as molecular motors to synthesize or hydrolyze ATP depending on the physiological conditions [7–9].

Some archaea and eubacteria contain an ATPase acting as a proton motive force-dependent ATP synthase [10,11]. Functional features and their general structures resemble F-type ATPases, whereas primary sequences of archaeal ATPases are closely related to eukaryotic V-type ATPases, which work as proton pumps depending on ATP hydrolysis in subcellular vesicles (Fig. 1C) [2,12]. The archaeal type ATPases are sometimes referred to as A-ATPases or V/A type ATPases [5,6,13], and these are regarded as an evolutionary origin of eukaryotic V-ATPases [14]. The V/A-ATPase from a thermophilic eubacterium *Thermus thermophilus* (*Tth*) is one of the best characterized rotary ATPases. The subunit composition of the *Tth* V/A-ATPase is similar to that of the eukaryotic enzyme; however, it has a simpler subunit structure and its physiological role is ATP synthesis *in vivo*, using energy from an electrochemical

◀ ***Significance*** ▶

ATP hydrolysis/synthesis in the soluble domain of proton-translocating rotary ATPases is coupled with proton flux across the membrane domain via a rotation of the common central rotor complex against the surrounding peripheral stator apparatus. Structures of the complete V/A type $H^+$-rotary ATPase have been revealed at a near atomic resolution level using cryogenic electron microscopy (cryo-EM). In this review article, we will describe the information about specimen preparation to improve the image quality and cryo-EM single particle analysis to overcome the intrinsic conformational heterogeneity of the *Tth* V/A-ATPases.

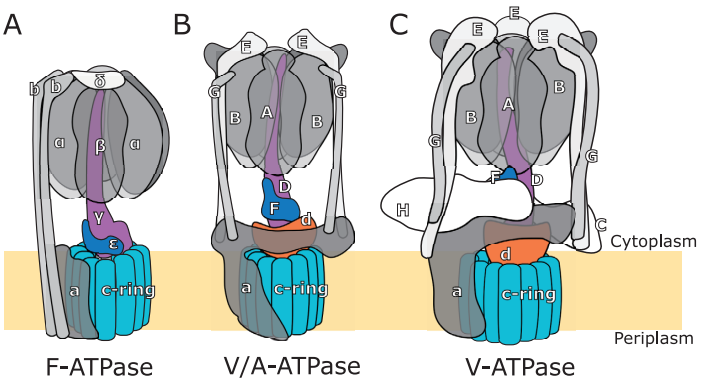


**Figure 1** Subunit arrangement in rotary ATPases. Schematic representations of bacterial F-type ATP synthase from *Bacillus* PS3 (A), V/A-type ATP synthase from *Thermus thermophilus* (B), and the yeast V-ATPase (C). F-type ATPases are found in the inner mitochondria membrane, in the thylakoid membrane of chloroplasts and in the bacterial plasma membrane, where they use proton gradient across the membrane to synthesize ATP. On the other hand, V-type ATPases were first purified from vacuoles, and work as proton pumps dependent on ATP hydrolysis. Colored rotor complexes of *B.* PS3 ($\gamma_1\varepsilon_1c_{10}$), *T. thermophilus* ($D_1F_1d_1c_{12}$) and the yeast ($D_1F_1d_1c_8c'_1c''_1$) rotate relative to the surrounding stator apparatus $\alpha_3\beta_3b_2a_1$, $A_3B_3E_2G_2a_1$ and $A_3B_3C_1E_3G_3H_1$ $a_1$, respectively.

potential generated by respiration to supply ATP to the cells [15]. The *Tth* V/A-ATPase is composed of subunits with a stoichiometry of $A_3B_3D_1E_2F_1G_2a_1c_{12}d_1$ (subunit numbers are written as a subscript) and has aqueous half proton channels in contact with a rotor complex (Fig. 1B, $D_1F_1d_1c_{12}$), which rotates relative to the surrounding stator apparatus (Fig. 1B, $A_3B_3E_2G_2a_1$). ATP is synthesized at the catalytic site in the AB pair when the rotor complex is driven by the proton motive force. Conversely, the rotor complex pumps protons through the membrane when ATP is hydrolyzed to ADP and $P_i$ at the catalytic site in the AB pair. The tip of the DF shaft interacts with a funnel shaped d-subunit, which forms a rotor complex with the $c_{12}$ ring, and their rotation results in proton translocation in membrane $V_o$ domain (Fig. 1). According to the dominant model of proton translocation in $V_o$, the a-subunit provides entry and exit of protons that protonate glutamate residues on the $c_{12}$ ring in contact with aqueous half channels [16]. In this model, the number of c-subunits in the $c_{12}$ ring is equal to the number of protons transported per revolution. Previous studies indicate that ATP-driven rotation of hydrophilic $V_1$ makes 120° steps, commensurate with the presence of three catalytic sites. The whole complex exhibits 30° steps for every proton translocation, which is consistent with the 12-fold symmetry of the $c_{12}$ ring [17]. The result indicates that the rotor-stator interaction of *Tth* V/A-ATPase is associated with proton translocation.

For the V/A-ATPase, X-ray crystallography has been used to determine partial structures of the central axis [18,19], peripheral stalk [20], membrane-embedded ring of c-subunits [21], hydrophilic domain of a-subunit [22], $A_3B_3$ hexamer [23], and soluble $V_1$ region [24]. Recent breakthroughs in structure analysis using cryogenic electron microscopy (cryo-EM) allowed us to determine the whole structure of rotary ATPases, including the F-type ATPase, V-ATPase, and V/A-ATPase [25–33]. In fact, the structure of the V/A-ATPase was revealed at a secondary structural level by Rubinstein's group in 2016 [13]. Despite the recent advances of structural studies using cryo-EM, high-resolution structures for understanding the mechanism of the V/A-ATPase in detail have not yet been obtained due to significant conformational heterogeneity of the rotary ATPases. In this review article, we describe the key points of cryo-EM grid preparation to obtain high-resolution membrane protein structures and single particle analysis of the *Tth* V/A-ATPase to overcome the intrinsic flexibility, which is necessary for the function.

## Sample preparation of *Tth* V/A-ATPase for single particle analysis

A key for *Tth* V/A-ATPases purification processes is the optimization of the solubilized conditions to generate monodispersed particles in solution. Membrane proteins are handled in solutions containing detergent above the critical micelle concentration (CMC) for their solubilization. However, the sample solution of detergent-solubilized membrane proteins contains detergent micelles and monomers, which increases the thickness of the amorphous ice by contributing a layered detergent at air-water interface of the specimen, resulting in decrease of the image contrast (Fig. 2A) [34,35]. To overcome this problem, lauryl maltose-neopentyl glycol (LMNG), a member of the maltose-neopentyl glycol class of amphipols, was used as a detergent to solubilize the ATPase [36]. LMNG and membrane proteins form a stable detergent-protein complex at a concentration even lower than CMC due to an extremely low off rate of LMNG from the membrane protein [37]. The removal of free detergent monomers and micelles from LMNG-solubilized samples improves the image contrast dramatically and enables acquisition of high-resolution data [27].

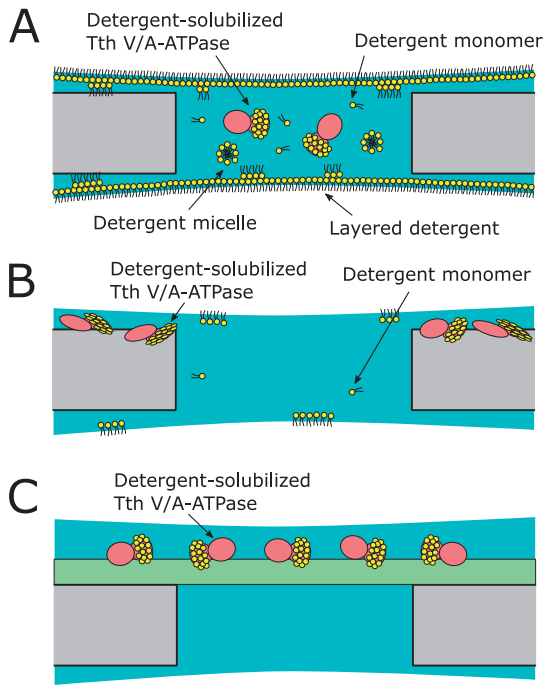


**Figure 2** Schematic representations of detergent-solubilized *Tth* V/A-ATPase on the cryo-grid in cryo-EM. Schematic representation of *Tth* V/A-ATPase existing with free detergent monomers, micelles, or layered detergent at the air-water interfaces when the complex is blotted on the holey carbon grid (A). Detergent-solubilized *Tth* V/A-ATPase mostly adsorbs to the supported carbon film (B). LMNG-solubilized *Tth* V/A-ATPase is immobilized on the carbon supported grid at a concentration lower than CMC. In this case, we can see lots of V/A-ATPase particles in the holes (C).

Another point for the cryo-grid preparation is that detergent-solubilized proteins tend to be adsorbed onto the surface of the carbon grid due to extensive glow discharged carbon surface. As a result, membrane protein particles are rarely found on the unsupported ice hole (Fig. 2B) [34,35]. This impels us to utilize membrane protein solutions at much higher concentrations than soluble proteins for the preparation of holey carbon cryo-grid. However, *Tth* V/A-ATPase particles were aggregated at high protein concentration on the unsupported ice hole. Conversely, a supporting carbon film has been used for cryo-grid preparation of ribosomes or membrane proteins [38,39]. The supporting carbon is capable of reducing charge-induced sample movement and provide an extra physical support for particle adsorption (Fig. 2C). When using the supported carbon cryo-grid, membrane protein particles appear to be concentrated on the carbon film, which enables to obtain many particle images at even low membrane protein concentration. For the *Tth* V/A-ATPase, the monodispersed particles were clearly observed on the supporting carbon film [27]. Nonetheless, this system contributes substantially to increasing background signal [40]. Recently, other materials have been attested as supporting films. For instance, graphene is an excellent support material because it is a one-atom thick (0.34 nm) hexagonal lattice of carbon atoms with high electronic conductivity properties [41,42]. We suppose that it may be possible to improve the resolution of the map of the *Tth* V/A-ATPase by using graphene oxide instead of carbon film.

As mentioned above, a number of methods have been developed to overcome obstacles to determine high-resolution membrane protein structures. Specimen preparation of membrane protein complexes for cryo-EM still is a key process to determine their high resolution cryo-EM structures.

## Single particle analysis of V/A-ATPases

Recent breakthroughs in structural studies using cryo-EM by improvements in the detector and image processing methods allowed for determination of the whole structure of rotary ATPases [13,27–33]. In 2015, the different rotational states of intact rotary ATPases were first observed in both the yeast V-ATPase and F-type ATP synthase, at 6–10 Å resolution, which has enabled a more detailed understanding of the molecular mechanism of these rotary motor proteins [28,29,33]. The resulting high-quality projection images of the ATPases made it possible to distinguish multiple conformational states during 3D classification [28,29]. However, resolving a high-resolution structure of the rotary ATPase has been extremely challenging because of their intrinsic conformational heterogeneity and instability.

Recently, our group determined the three rotational state structures of *Tth* V/A-ATPase, based on the orientation of the central rotor subunit (Fig. 3A) [27]. The position of the central rotor subunits was different for each state, that was closely matched 120° steps which occurred during the ATP hydrolysis of $V_1$. The EM structure corresponding to state 1 composed of major class gave a 5 Å resolution map, which is higher than previous reports for the V/A-ATPase structure at that time. This cryo-EM density map provided evidence for integrity of the V/A-ATPase against internal rotation of rotor part relative to stator. Close interactions between EG-subunits and B-subunits in $V_1$ are identified, which appear to form rigid β sheet structures (Fig. 3B, C). This interaction is consistent with our results of previous reconstitution assay, showing that the $A_3B_3$ of the V/A-ATPase is tightly associated with the two peripheral stalks [43]. Additionally, interface structures of the central rotor subunits indicated the specific interactions among the rotor subunits in the complex (Fig. 3D). The interaction surface was identified between the short helix region of the D-subunit and the d-subunit cavity, suggesting an important interaction for appropriate fitting in our previous studies [44]. Tight electrostatic interactions between the two inner helices of the $c_{12}$ ring and the N-terminal helix of the d-subunit are also clearly observed (Fig. 3E). We suppose that the robustness of the rotor complex during rotation relative to the stator is maintained by the interaction between the d- and the $c_{12}$ ring in the *Tth* V/A-ATPase.

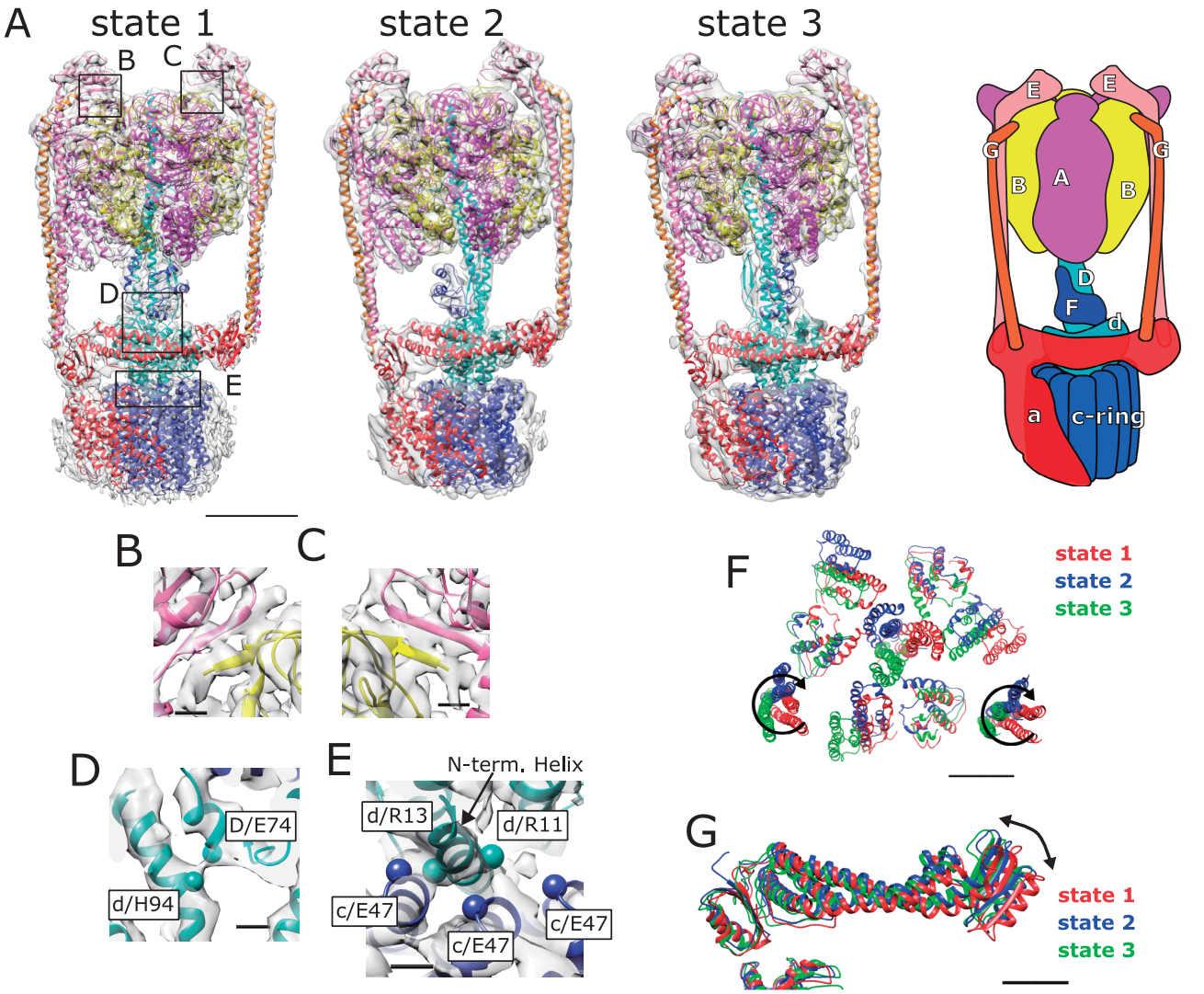


**Figure 3** Three rotational states of *Tth* V/A-ATPase. Cryo-EM maps of three different conformational states fitting atomic models of the subunits from *Tth* V/A-ATPase, respectively (A). A schematic model of *Tth* V/A-ATPase is shown on the right. Colors of the subunits displayed in the schematic model correspond to the colors of the subunits in atomic models fitted into the maps of *Tth* V/A-ATPase. Scale bar, 50 Å. Magnified views of interface structures between B- and E-subunit (B, C), d- and D-subunit (D) and d- and $c_{12}$ ring (E) in state1 are indicated respectively. The positions of glutamate residue on the D-subunit (E74) and the histidine residue on the d-subunit (H94) are indicated by sphere format (D). The positions of the glutamate on the c-subunit (E47) and the arginine on the d-subunit (R11, R13) are shown in sphere format (E). The N-terminal helix of the d-subunit is indicated by an arrow in E. Scale bar, 5 Å. The viewing positions of B-E are indicated as squares in A. Circular motions of EG subunits during transition of three rotational states (F). Bottom views of the N-terminal region of the EG-subunits are indicated when three states structures are superimposed at the N-terminal β barrel domain of B-subunit. Colors corresponding to the state1, state2 and state3 are red, blue and green, respectively. Circular motion of EG subunits are indicated by arrows. Scale bar, 30 Å. Comparison of the N-terminal domain of the a-subunit in three states when subunits are superimposed at the C-terminal domain of the a-subunit (G). The color of each state corresponds to F. Up-and-down motion of the N-terminal domain of a-subunit in three states is indicated by an arrowhead. Scale bar, 20 Å. Model IDs corresponding to the rotational states of *Tth* V/A-ATPase are 5Y5X and EMDB-6810 for state1, 5Y5Z and EMDB-6812 for state2, and 5Y60 and EMDB-6813 for state3.

The three different structures provided insights into the rotation of the whole complex, which allowed to estimate the movement of each subunit during the rotation. The remarkably different conformation of the EG stalk region was observed in the three states, though superposition of the β barrel domain of the B-subunit attached to the peripheral stalk revealed no apparent difference in the globular region. A circular motion of the peripheral stalks is indicated among the three rotational states on the pivot point of the coiled-coil domain of the stalk regions in each state (Fig. 3F). With the circular movement of the EG stalk region, the N-terminal region of the a-subunit moves up-and-down at the linkage to the C-terminal region (Fig. 3G). The conformational changes in the stator subunits in the three rotational states is visible in Supplementary Movie 1 of our article [27]. This movement of the stator subunits in *Tth* V/A-ATPase is modestly com-

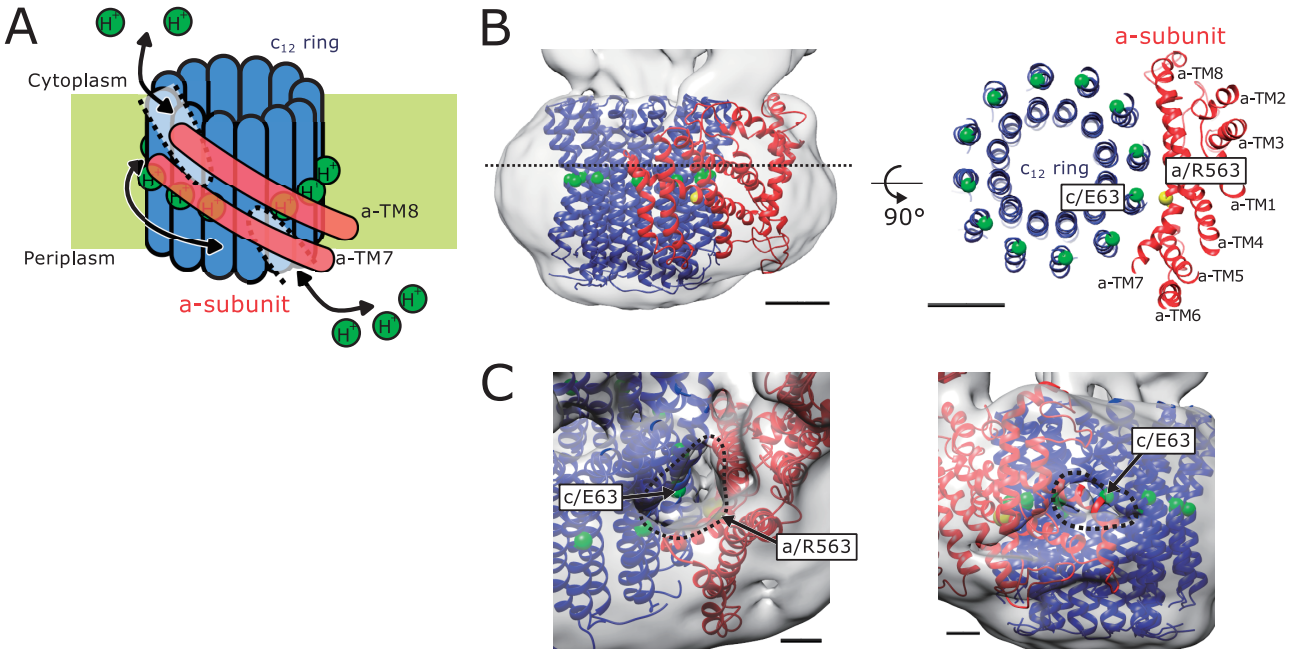


**Figure 4** Structure of the membrane embedded domain of *Tth* V/A-ATPase. Two-channel model of proton translocation of *Tth* V/A-ATPase (A). Proton translocation occurs through the periplasmic and cytoplasmic pores shown by dotted lines. A part of the a-subunit colored in transparent magenta is indicated in (A), showing the important two transmembrane helices (a-TM7, a-TM8). Density map colored semi-transparent gray is fitted atomic model of state 1 (PDB ID; 5Y5X) with the detergent shell surrounding the $V_o$ (B). A top view of contact surface between the $c_{12}$ ring and the a-subunit at cytoplasmic pore is shown in right. Spheres representing the essential residues of the arginine on the transmembrane helix 7 of the a-subunit and the glutamate residues on the $c_{12}$ ring are colored yellow and green, respectively. Scale bar, 20 Å. Close-up views from the cytoplasmic (above) and periplasmic (below) side (C). Density map colored semi-transparent gray shows large cavities outlined in black. Spheres showing the essential residues of the arginine on the transmembrane helix 7 of the a-subunit and the glutamate residues on the $c_{12}$ ring are colored yellow and green, respectively. Scale bar, 10 Å.

pared to that of the yeast V-ATPase [28]. The models of the three rotational states of yeast V-ATPase showed the sliding motion of the three EG stalks and the shaking motion of the hydrophilic region of the a-subunit [27,28]. These conformational changes may imply that the flexibility of the stator plays an essential role in storing torsional energy during rotation in rotary ATPases.

It is suggested that rotary ATPases are coupled with the catalytic and membrane embedded regions to transmit torque between ATP hydrolysis/synthesis and proton translocation [45,46]. We previously provided evidence that 12 dwell positions per revolution was observed by rotational assay when the intact *Tth* V/A-ATPase hydrolyzes ATP [17]. Possibly, free energy lost by ATP hydrolysis in $V_1$ provides the energy slope to adopt the mechanical event of the ~30° steps in the direction of rotation. We suppose that the flexibility of the stator apparatus plays an important role in the elasticity of the protein allowing accommodation of these 30° movements.

## The membrane-embedded domain

The dominant model for how the a-subunit translocates protons is proposed as two aqueous half channels, each extending to the middle of the lipid bilayer [2,5,6]. According to the model, the a-subunit provides entry and exit of protons that protonate glutamate residues on the $c_{12}$ ring in contact with aqueous half channels (Fig. 4A). The EM structure of the membrane-embedded region of the V/A-ATPase provided a higher resolution structure of $a_1c_{12}$ region than previous intact rotary ATPase structures at that time, and enabled the main chains of the a-subunit and the $c_{12}$ ring to fit well into the EM map [27]. The two highly tilted α helices of the a-subunit and the adjacent four outer α helices of $c_{12}$ ring were clearly identified in the model. The highly conserved arginine residue (R563) was positioned in the central region of the transmembrane helix 7 of the a-subunit (a-TM7), where the a-subunit was in close proximity to the outer helices of c-subunit (Fig. 4B). Homology mapping suggested that the conserved R563 on the a-subunit was positioned close to the conserved E63 on the c-subunit (Fig. 4B), which are necessary for proton pumping activity in yeast [47,48]. The cryo-EM map of state 1 with solvent density showed that the detergent shell was recessed at each side of the membrane to form two aqueous cavities (Fig. 4C). The cytoplasmic aqueous cavity provides direct access to the hydrophilic residues on the a-TM7, reaching the conserved Arg-Glu residue pair at the interface of the a-TM7 and the outer helix of c-subunit (Fig. 4B), indicating that the cavity corresponds to the cytoplasmic half channel. The peri-

plasmic cavity faces the helix bundle composed of a-TM1, a-TM2, and a-TM3, including a line of hydrophilic residues, and connects to the aqueous hole giving access to the tilted helices.

## Perspective

Future work will be focused on obtaining a higher resolution cryo-EM map of *Tth* V/A-ATPase to reveal the mechanism by which proton translocation across the $V_o$ channel powers the rotation of the rotor ring. Therefore, clearer EM images of V/A-ATPase single particles are necessary to obtain higher resolution structures, which will enable us to determine the accurate orientation of water molecules in the $V_o$ channels. As mentioned above, methodologies for both sample and cryo-grid preparation of membrane proteins have been developed by several groups. A nanodisc is a powerful tool for the removal of detergents which tend to decrease cryo-image contrast [32,49,50]. Additionally, series of new class of amphipol are available for cryo-grid preparation to obtain clearer cryo-micrographs [31,51,52]. Methodologies of grid preparation have also been improved by using a new material [53–56]. Gold grids nearly eliminate radiation-induced deformation of ice-embedded specimens, resulting in the prevention of specimen movement during irradiation. The use of gold grids will improve data quality for specimens [55,56], which will increase the accuracy of 3D classification criteria for *Tth* V/A-ATPase and enable the classification of more detailed rotational states of *Tth* V/A-ATPase; for example, those corresponding to 30° steps associated with proton translocation [17].

## Acknowledgments

We are grateful to all the members of our lab for their continuous support and technical assistance. Our research is supported in part by the Nanotechnology Hub and by Grants-in-Aid from the Ministry of Education, Science and Culture of Japan to K. Y. (No 17H03648), and J. K. (No. 16K21472).

## Conflicts of interest

A. N., J. K., K. M., and K. Y declare that they have no conflict of interest.

## Author Contribution

A. N., J. K., K. M., and K. Y wrote the paper.

## References

[1] Yoshida, M., Muneyuki, E. & Hisabori, T. ATP synthase—a marvellous rotary engine of the cell. *Nat. Rev. Mol. Cell Biol.* **2**, 669–677 (2001).
[2] Forgac, M. Vacuolar ATPases: rotary proton pumps in physiology and pathophysiology. *Nat. Rev. Mol. Cell Biol.* **8**, 917–929 (2007).
[3] Yokoyama, K. & Imamura, H. Rotation, structure, and classification of prokaryotic V-ATPase. *J. Bioenerg. Biomembr.* **37**, 405–410 (2005).
[4] Imamura, H., Nakano, M., Noji, H., Muneyuki, E., Ohkuma, S., Yoshida, M., *et al.* Evidence for rotation of $V_1$-ATPase. *Proc. Natl. Acad. Sci. USA* **100**, 2312–2315 (2003).
[5] Mazhab-Jafari, M. T. & Rubinstein, J. L. Cryo-EM studies of the structure and dynamics of vacuolar-type ATPases. *Sci. Adv.* **2**, e1600725 (2016).
[6] Kühlbrandt, W. & Davies, K. M. Rotary ATPases: A New Twist to an Ancient Machine. *Trends. Biochem. Sci.* **41**, 106–116 (2016).
[7] Kobayashi, H. A proton-translocating ATPase regulates pH of the bacterial cytoplasm. *J. Biol. Chem.* **260**, 72–76 (1985).
[8] Kakinuma, Y. & Igarashi, K. Purification and characterization of the catalytic moiety of vacuolar-type $Na^+$-ATPase from *Enterococcus hirae*. *J. Biochem.* **116**, 1302–1308 (1994).
[9] Kakinuma, Y., Yamato, I. & Murata, T. Structure and function of vacuolar $Na^+$-translocating ATPase in *Enterococcus hirae*. *J. Bioenerg. Biomembr.* **31**, 7–14 (1999).
[10] Yokoyama, K., Oshima, T. & Yoshida, M. *Thermus thermophilus* membrane-associated ATPase. Indication of a eubacterial V-type ATPase. *J. Biol. Chem.* **265**, 21946–21950 (1990).
[11] Mukohata, Y. & Yoshida, M. The $H^+$-translocating ATP synthase in *Halobacterium halobium* differs from $F_0F_1$-ATPase/synthase. *J. Biochem.* **102**, 797–802 (1987).
[12] Cotter, K., Stransky, L., McGuire, C. & Forgac, M. Recent Insights into the Structure, Regulation, and Function of the V-ATPases. *Trends Biochem. Sci.* **40**, 611–622 (2015).
[13] Schep, D. G., Zhao, J. & Rubinstein, J. L. Models for the a subunits of the *Thermus thermophilus* V/A-ATPase and *Saccharomyces cerevisiae* V-ATPase enzymes by cryo-EM and evolutionary covariance. *Proc. Natl. Acad. Sci. USA* **113**, 3245–3250 (2016).
[14] Gogarden, J. P., Kibak, H., Dittrich, P., Taiz, L., Bowman, E. J., Manolson, M. F., *et al.* Evolution of the vacuolar $H^+$-ATPase: implication for the origin of eukaryotes. *Proc. Natl. Acad. Sci. USA* **86**, 6661–6665 (1989).
[15] Nakano, M., Imamura, H., Toei, M., Tamakoshi, M., Yoshida, M. & Yokoyama, K. ATP hydrolysis and synthesis of a rotary motor V-ATPase from *Thermus thermophilus*. *J. Biol. Chem.* **283**, 20789–20796 (2008).
[16] Junge, W., Lill, H. & Engelbrecht, S. ATP synthase: an electrochemical transducer with rotatory mechanics. *Trends. Biochem. Sci.* **22**, 420–423 (1997).
[17] Furuike, S., Nakano, M., Adachi, K., Noji, H., Kinoshita, K. Jr. & Yokoyama, K. Resolving stepping rotation in *Thermus thermophilus* $H^+$-ATPase/synthase with an essentially drag-free probe. *Nat. Commun.* **2**, 233 (2011).
[18] Iwata, M., Imamura, H., Stambouli, E., Ikeda, C., Tamakoshi, M., Nagata, K., *et al.* Crystal structure of a central stalk subunit C and reversible association/dissociation of vacuole-type ATPase. *Proc. Natl. Acad. Sci. USA* **101**, 59–64 (2004).
[19] Makyio, H., Iino, R., Ikeda, C., Imamura, H., Tamakoshi, M., Iwata, M., *et al.* Structure of a central stalk subunit F of prokaryotic V-type ATPase/synthase from *Thermus thermophilus*. *EMBO J.* **24**, 3974–3983 (2005).
[20] Lee, L. K., Stewart, A. G., Donohoe, M., Bernal, R. A. & Stock, D. The structure of the peripheral stalk of *Thermus thermophilus* $H^+$-ATPase/synthase. *Nat. Struct. Mol. Biol.* **17**, 373–378 (2010).
[21] Murata, T., Yamato, I., Kakinuma, Y., Leslie, A. G. & Walker, J. E. Structure of the Rotor of the V-Type $Na^+$-ATPase from *Enterococcus hirae*. *Science* **308**, 654–659 (2005).
[22] Srinivasan, S., Vyas, N. K., Baker M. L. & Quiocho, F. A.

Crystal structure of the cytoplasmic N-terminal domain of subunit I, a homolog of subunit a, of V-ATPase. *J. Mol. Biol.* **412**, 14–21 (2011).
[23] Maher, M. J., Akimoto, S., Iwata, M., Nagata, K., Hori, Y., Yoshida, M., *et al.* Crystal structure of $A_3B_3$ complex of V-ATPase from *Thermus thermophilus*. *EMBO J.* **28**, 3771–3779 (2009).
[24] Nagamatsu, Y., Takeda, K., Kuranaga, T., Numoto, N. & Miki, K. Origin of Asymmetry at the Intersubunit Interfaces of $V_1$-ATPase from *Thermus thermophilus*. *J. Mol. Biol.* **425**, 2699–2708 (2013).
[25] Scheres, S. H. RELION: implementation of a Bayesian approach to cryo-EM structure determination. *J. Struct. Biol.* **180**, 519–530 (2012).
[26] Li, X., Mooney, P., Zheng, S., Booth, C. R., Braunfeld, M. B., Gubbens, S., *et al.* Electron counting and beam-induced motion correction enable near-atomic-resolution single-particle cryo-EM. *Nat. Methods* **10**, 584–590 (2013).
[27] Nakanishi, A., Kishikawa, J., Tamakoshi, M., Mitsuoka, K. & Yokoyama, K. Cryo EM structure of intact rotary $H^+$-ATPase/synthase from *Thermus thermophilus*. *Nat. Commun.* **9**, 89 (2018).
[28] Zhao, J., Benlekbir, S. & Rubinstein, J. L. Electron cryomicroscopy observation of rotational states in a eukaryotic V-ATPase. *Nature* **521**, 241–245 (2015).
[29] Zhou, A., Rohou, A., Schep, D. G., Bason, J. V., Montgomery, M. G., Walker, J. E., *et al.* Structure and conformational states of the bovine mitochondrial ATP synthase by cryo-EM. *Elife* **4**, e10180 (2015).
[30] Sobti, M., Smits, C., Wong, A. S., Ishmukhametov, R., Stock, D., Sandin, S., *et al.* Cryo-EM structures of the autoinhibited *E. coli* ATP synthase in three rotational states. *Elife* **5**, e21598 (2016).
[31] Guo, H., Suzuki, T. & Rubinstein, J. L. Structures of a bacterial ATP synthase. *Elife* **8**, e43128 (2019).
[32] Hahn, A., Vonck, J., Mills, D. J., Meier, T. & Kühlbrandt, W. Structure, mechanism, and regulation of the chloroplast ATP synthase. *Science* **360**, (2018).
[33] Allegretti, M., Klusch, N., Millls, D. J., Vonck, J., Kühlbrandt, W. & Davies, K. M. Horizontal membrane-intrinsic α helices in the stator a-subunit of an F-type ATP synthase. *Nature* **521**, 237–240 (2015).
[34] Rubinstein, J. L. Structural analysis of membrane protein complexes by single particle electron microscopy. *Methods* **41**, 409–416 (2007).
[35] Schmidt-Krey, I. & Rubinstein, J. L. Electron cryomicroscopy of membrane proteins: specimen preparation for two-dimensional crystals and single particles. *Micron* **42**, 107–116 (2011).
[36] Chae, P. S., Rasmussen, S. G., Rana, R. R., Gotfryd, K., Chandra, R., Goren, M. A., *et al.* Maltose-neopentyl glycol (MNG) amphiphiles for solubilization, stabilization and crystallization of membrane proteins. *Nat. Methods* **7**, 1003–1008 (2010).
[37] Hauer, F., Gerle, C., Fischer, N., Oshima, A., Shinzawa-Itoh, K., Shimada, S., *et al.* GraDeR: Membrane Protein Complex Preparation for Single-Particle Cryo-EM. *Structure* **23**, 1769–1775 (2015).
[38] Frank, J., Penczek, P., Agrawal, R. K., Grassucci, R. A. & Heagle, A. B. Three-dimensional cryoelectron microscopy of ribosomes. *Methods Enzymol.* **317**, 276–291 (2000).
[39] Rubinstein, J. L. & Walker, J. ATP synthase from *Saccharomyces cerevisiae*: location of the OSCP subunit in the peripheral stalk region. *J. Mol. Biol.* **321**, 613–619 (2002).
[40] Zhao, M., Wu, S., Zhou, Q., Vivona, S., Cipriano, D. J., Cheng, Y., *et al.* Mechanistic insights into the recycling machine of the SNARE complex. *Nature* **518**, 61–67 (2015).
[41] Pantelic, R. S., Meyer, J. C., Kaiser, U., Baumeister, W. & Plitzko, J. M. Graphene oxide: a substrate for optimizing preparations of frozen-hydrated samples. *J. Struct. Biol.* **170**, 152–156 (2010).
[42] Palovcak, E., Wang, F., Zheng, S. Q., Yu, Z., Li, Z., Betegon, M., *et al.* A simple and robust procedure for preparing graphene-oxide cryo-EM grids. *J. Struct. Biol.* **204**, 80–84 (2018).
[43] Kishikawa, J. & Yokoyama, K. Reconstitution of Vacuolar-type Rotary $H^+$-ATPase/Synthase from *Thermus thermophilus*. *J. Biol. Chem.* **287**, 24597–24603 (2012).
[44] Nakanishi, A., Kishikawa, J., Tamakoshi, M. & Yokoyama, K. The ingenious structure of central rotor apparatus in $V_oV_1$; key for both complex disassembly and energy coupling between $V_1$ and $V_o$. *PLoS One* **10**, e0119602 (2015).
[45] Mitome, N., Suzuki, T., Hayashi, S. & Yoshida, M. Thermophilic ATP synthase has a decamer c-ring: indication of non-integer 10:3 $H^+$/ATP ratio and permissive elastic coupling. *Proc. Natl. Acad. Sci. USA* **101**, 12159–12164 (2004).
[46] Wächter, A., Bi, Y., Dunn, S. D., Cain, B. D., Sielaff, H., Wintermann, F., *et al.* Two rotary motors in F-ATP synthase are elastically coupled by a flexible rotor and a stiff stator stalk. *Proc. Natl. Acad. Sci. USA* **108**, 3924–3929 (2011).
[47] Hirata, R., Graham, L. A., Takatsuki, A., Stevens, T. H. & Anraku, Y. VMA11 and VMA16 encode second and third proteolipid subunits of the Saccharomyces serevisiae vacuolar membrane $H^+$-ATPase. *J. Biol. Chem.* **272**, 4795–4803 (1997).
[48] Kawasaki-Nishi, S., Nishi, T. & Forgac, M. Arg-735 of the 100-kDa subunit a of the yeast V-ATPase is essential for proton translocation. *Proc. Natl. Acad. Sci. USA* **98**, 12397–12402 (2001).
[49] Schuler, M. A., Denisov, I. G. & Sligar, S. G. Nanodiscs as a new tool to examine lipid-protein interactions. *Methods Mol. Biol.* **974**, 415–433 (2013).
[50] Roh, S. H., Stam, N. J., Hryc, C. F., Couoh-Cardel, S., Pintilie, G., Chiu, W., *et al.* The 3.5-Å CryoEM Structure of Nanodisc-Reconstituted Yeast Vacuolar ATPase Vo Proton Channel. *Mol. Cell* **69**, 993–1004 (2018).
[51] Chae, P. S., Rasmussen, S. G., Rana, R. R., Gotfryd, K., Kruse, A. C., Manglik, A., *et al.* A new class of amphiphiles bearing rigid hydrophobic groups for solubilization and stabilization of membrane proteins. *Chemistry* **18**, 9485–9490 (2012).
[52] Mazhab-Jafari, M. T., Rohou, A., Schmidt, C., Bueler, S. A., Benlekbir, S., Robinson, C. V., *et al.* Atomic model for the membrane-embedded $V_O$ motor of a eukaryotic V-ATPase. *Nature* **539**, 118–122 (2016).
[53] Llaguno, M. C., Xu, H., Shi, L., Huang, N., Zhang, H., Liu, Q., *et al.* Chemically functionalized carbon films for single molecule imaging. *J. Struct. Biol.* **185**, 405–417 (2014).
[54] Kelly, D. F., Dukovski, D. & Walz, T. Monolayer purification: a rapid method for isolating protein complexes for single-particle electron microscopy. *Proc. Natl. Acad. Sci. USA* **105**, 4703–4708 (2008).
[55] Russo, C. J. & Passmore, L. A. Progress towards an optimal specimen support for electron cryomicroscopy. *Curr. Opin. Struct. Biol.* **37**, 81–89 (2016).
[56] Russo, C. J. & Passmore, L. A. Electron microscopy: Ultrastable gold substrates for electron cryomicroscopy. *Science* **346**, 1377–1380 (2014).